Characterization of Jason-3 Spacecraft Surface Charging in LEO Polar Regions From AMBER Observations

Florine Enengl, Mika K. G. Holmberg, Fabrice Cipriani, Jean-André Sauvaud, Denis Payan, Jean-Charles Matéo-Vélez, Angelica Sicard, and Benoît Lavraud

***Abstract*— We have characterized spacecraft charging events in low Earth orbit (LEO) polar regions with the Active Monitor Box of Electrostatic Risk (AMBER) instrument onboard the Joint Altimetry Satellite Oceanography Network—3 (Jason-3) ocean topography mission for the first time for this spacecraft. AMBER data, taken at an altitude of 1336 km, over the period January 2017–March 2020, with measurements recorded close to the current solar minimum have been analyzed, using systematic filtering of ions spectrograms with selected threshold energies and time windows to detect negative spacecraft charging events; 109 spacecraft charging events were found. The events are examined visually and characterized by their spatial and temporal location, duration, and intensity (e.g., spacecraft potential). At the Jason-3 altitude (1336 km), the ion signature predominately lasts under 30 s in conjunction with auroral inverted V crossings, while intense fluxes of electrons corresponding to the encounter of the discrete auroral region last between 30 s and 1 min. Most of the detected spacecraft charging events show charging levels between −30 and −1000 V. The spacecraft charging events are located in the magnetic local time (MLT) sector 17h–05h, predominately before midnight. The distribution is equal between the northern and southern hemispheres. We found a high correlation between the charging time profile and that of the auroral electron average energy and energy flux along the satellite path. Overall statistics over three years as well as different event morphologies, electron spectra, and comparisons to worst case electron flux spectral distributions are presented and discussed.**

Manuscript received September 30, 2021; revised February 14, 2022; accepted February 21, 2022. Date of publication April 6, 2022; date of current version April 11, 2022. The review of this article was arranged by Senior Editor S. Lai. *(Corresponding author: Florine Enengl.)*

Florine Enengl was with the Space Environments and Effects Section (TEC-EPS), European Space Agency, 2201 AG Noordwijk, The Netherlands. She is now with the Department of Physics, University of Oslo, 0315 Oslo, Norway (e-mail: florine.enengl@fys.uio.no).

Mika K. G. Holmberg was with the Space Environments and Effects Section (TEC-EPS), European Space Agency, 2201 AG Noordwijk, The Netherlands. She is now with the Planetary Magnetospheres Research Group, School of Cosmic Physics, Dublin Institute for Advanced Studies, Dublin 15, Ireland.

Fabrice Cipriani is with the Space Environments and Effects Section (TEC-EPS), European Space Agency, 2201 AG Noordwijk, The Netherlands.

Jean-André Sauvaud and Benoît Lavraud are with the Institut de Recherche en Astrophysique et Planétologie (IRAP), 31400 Toulouse, France.

Denis Payan is with the Centre Nationale d'Etudes Spatiales, 31400 Toulouse, France.

Jean-Charles Matéo-Vélez and Angelica Sicard are with ONERA—The French Aerospace Lab, 91120 Toulouse, France.

This article has supplementary material provided by the authors and color versions of one or more figures available at https://doi.org/10.1109/TPS.2022.3157958.

Digital Object Identifier 10.1109/TPS.2022.3157958

***Index Terms*— Low Earth orbit (LEO) auroral environment, plasma spectrometer, spacecraft charging.**

I. Introduction

A SPACECRAFT located in a plasma will be charged by the constant bombardment of electrons and ions. Additional currents to the spacecraft, such as photoelectrons produced by UV and secondary electrons being knocked out by the impacting electrons and ions, also contribute to the electrostatic potential of the spacecraft (for a review, see [1]). Low altitude high inclination spacecraft, such as meteorological and Earth observation satellites, are subject to transient auroral energetic particle fluxes, which may lead to substantial spacecraft charging. Multiple studies have been made to characterize the spatial and temporal distribution of charging events of the Freja (located at 600–1800 km altitude) and DMSP (811–853 km) satellites. In this article, we are, for the first time, evaluating frame charging of the Joint Altimetry Satellite Oceanography Network—3 (Jason-3) (1336 km altitude) satellite.

Gussenhoven *et al.* [2] (DMSP), Wahlund *et al.* [3] (Freja), Anderson [4] (DMSP), and Meng *et al.* [5] (DMSP) suggested that charging conditions are met during intense energetic electron precipitation events linked to auroral arcs, in a region of locally depleted thermal plasma density (at most 10^4 cm^{-3}) predominately on the nightside region, i.e., in the absence of UV radiation. Note that from rocket and satellite observations, it was indeed revealed that auroral electrons show nearly monoenergetic peaks around 1–10 keV in their energy spectra. Their peak energy is initially low and increases with time and finally decreases on the energy time (E–t) spectrograms. Frank and Ackerson [6] referred to their λ shaped structures as inverted-V electrons.

Gussenhoven *et al.* [2], Anderson [4], and Meng *et al.* [5] used particle and plasma measurements from two polar-orbiting satellites, DMSP F6 and F7, to investigate severe spacecraft charging, and found that the magnitude of the potential difference between a spacecraft and the ambient plasma exceeds −100 V if three conditions are met: the satellite must be: 1) in darkness; 2) in an intense energetic electron precipitation event that produces a bright auroral arc; and 3) in a region of locally depleted thermal plasma density. This combination has been found very short-lived,

with a duration of tens of seconds or over a spatial extent of 10–100 km. Negative spacecraft frame charging has been found down to levels of −462 V. It must be noted that Frooninckx and Sojka [7] performing an analysis of DMSP F6, F7, F8, and F9 satellites concluded that charging is most frequent during solar minimum. A large analysis of statistical occurrence of charging events in the altitude range 1000–1800 km in the northern hemisphere on the polar (high latitude) orbiting Freja satellite was carried out by Wahlund *et al.* [3]. The analysis showed that Freja charging events are associated with energetic electron precipitation and concludes that the energetic electrons above a few keV are the direct cause for most Freja charging events. An 11-year study of the DMSP spacecraft (at 840 km, circular orbits) from [4] presents over 1600 charging events, for spacecraft charging levels exceeding −100 V during an auroral zone crossing. Anderson [4] stated that charging events experienced by the DMSP were all associated with auroral arcs. A correlation to the 11-year solar cycle was found, with the largest number of events during solar minimum, due to a low background thermal plasma density lower than 10^4 cm^{-3}. The authors state that the primary driver for the occurrence frequency of charging events on the DMSP spacecraft and the solar cycle dependence is the requirement that the ambient density must be below about 10^4 cm^{-3}. The findings are in agreement with [2], [3], and [8].

We here present a survey of Jason-3/Active Monitor Box of Electrostatic Risk (AMBER) data. Filtering the ion spectrogram using the ion peak method, described in Section III, provides us with a set of spacecraft charging events that are used for a statistical study of their characteristics, such as spatial and temporal location, duration, and intensity. While the charging risk encountered on low Earth orbit (LEO) high inclination orbits, which can span over a large range of altitudes, is reasonably well recognized by spacecraft designers, its assessment still relies on a fairly limited description of the environment, e.g., in terms of statistical variability. The applicability of current engineering standards is solely relying on DMSP-based spectral characteristics. Therefore, considering this new dataset brings complementary information to current auroral environment descriptions. We show here that the spacecraft charging time profile closely follows the time profile of the electron average energy and the electron energy flux, thus opening the possibility to predict charging events from a model of discrete auroral precipitation. The ultimate aim of this kind of study would be, in the future, to be able to predict spacecraft charging from magnetic indices deduced from solar wind parameters obtained in the solar wind at the L1 location, index-dependent auroral precipitation characteristics, and the satellite orbital parameters.

II. Spacecraft and Instrument

The Jason-3 is a three-axis stabilized spacecraft. It was launched on January 17, 2016 on a nearly circular orbit at 1336 km altitude and 66° inclination. The onboard AMBER is a double-head top-hat thermal electron and ion electrostatic analyzer [9]. This double top-hat instrument is designed to measure magnetospheric thermal ion and electron populations and to monitor spacecraft electrostatic charging. Instrument descriptions can be found in [10] and [11]. Prospective developments of this instrument are described in [9]. AMBER measures electrons and ions in the 10 eV–30 keV energy range. The field of view of both spectrometers is 180° × 6° centered on the zenith. The 180° field of view is divided into four sectors: the two central ones (sectors 2 and 3) measure precipitating particles, while the two side ones (sectors 1 and 4) record nearly trapped or upstreaming particles. The AMBER spectrometers provide particle spectra with a maximum of 128 energy steps. However, 32 or 16 energy steps and a time resolution of either 0.5 or 2 s are the most common instrument modes. The 32 energy channels are shown in Table I. The 16 channel resolution combines two energy channels at a time (channels 1 and 2, 3 and 4, 5 and 6, and so on). The raw data are given in counts [#], which is directly proportional to the energy flux, except during the charging event.

TABLE I
List of the AMBER Ion and Electron Energy Channels

ion channels			electron channels		
#	E_{min} [eV]	E_{max} [eV]	#	E_{min} [eV]	E_{max} [eV]
1	10	12.65	1	10	12.63
2	12.65	16.25	2	12.63	16.19
3	16.25	20.88	3	16.19	20.76
4	20.88	26.83	4	20.76	26.62
5	26.83	34.47	5	26.62	34.13
6	34.47	44.28	6	34.13	43.77
7	44.28	56.89	7	43.77	56.12
8	56.89	73.09	8	56.12	71.95
9	73.09	93.90	9	71.95	92.27
10	93.90	120.64	10	92.27	118.31
11	120.64	154.99	11	118.31	151.69
12	154.99	199.13	12	151.69	194.50
13	199.13	255.85	13	194.50	249.40
14	255.85	328.71	14	249.40	319.80
15	328.7	422.32	15	319.80	410.07
16	422.32	542.59	16	410.07	525.81
17	542.59	697.10	17	525.81	674.22
18	697.10	895.63	18	674.22	864.53
19	895.63	1150.69	19	864.53	1108.54
20	1150.69	1478.38	20	1108.54	1421.44
21	1478.38	1899.40	21	1421.44	1822.63
22	1899.40	2440.31	22	1822.63	2337.08
23	2440.31	3135.27	23	2337.08	2996.73
24	3135.27	4028.14	24	2996.73	3842.57
25	4028.14	5175.28	25	3842.57	4927.15
26	5175.28	6649.11	26	4927.15	6317.86
27	6649.11	8542.65	27	6317.86	8101.08
28	8542.65	10975.44	28	8101.08	10387.64
29	10975.44	14101.05	29	10387.64	13319.58
30	14101.05	18116.77	30	13319.58	17079.09
31	18116.77	23276.11	31	17079.09	21899.72
32	23276.11	29440	32	21899.72	27648

III. Filtering the Ion Spectrogram

To detect the spacecraft charging events, an automatic event detection method was developed from visual inspection of a handful of known Jason-3 charging events. All charging events are detected in the ion spectrum, as they are easier to detect than in the electron spectrum. The charging is produced by the change in the electron energy distribution, and this change can also be detected in the ion spectrum. If the increase in any of the ion energy levels is above $10^{2.9}$# (which corresponds to an approximate energy flux of 3.34×10^5 eV cm^{-2}s^{-1}sr^{-1}eV^{-1}) over three consecutive measurement spectra and associated with an increase in the average electron energy above 4 keV, the event was classified as a spacecraft charging event.

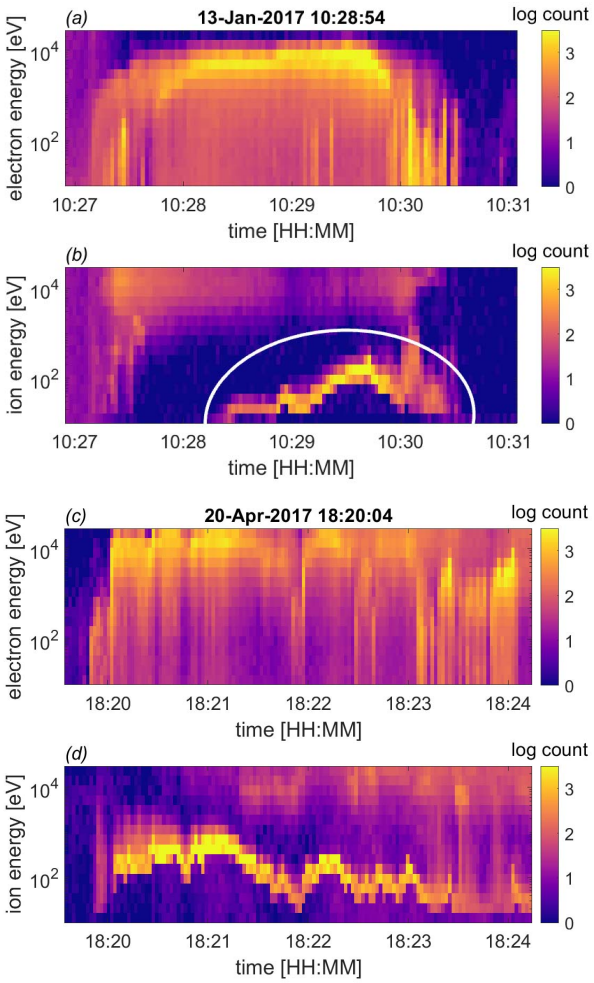

Fig. 1. (a) and (c) Electron and (b) and (d) ion energy-time spectrograms showing count rates versus energy and time. The count rate values are color-coded. (a) and (b) Typical spacecraft charging event with the ion signature highlighted with a white ellipse. (c) and (d) Spacecraft charging event with the longest observed ion signature.

For each event detected, an afterward visual inspection was carried out in order to determine whether a given event could correspond to actual charging of the platform or to a natural environment signature not affecting the platform electrostatic potential. This was in order to exclude for instance phenomena such as ion injections (as reported, e.g., in [11]) and natural, drift induced, quasi-monoenergetic ion structures that are not accompanied by high-energy electrons. The visual selection was aided by the description of typical spectral fluxes corresponding to particles precipitation, cusp particles, and spacecraft charging events carried out in "preliminary results of the AMBER particles measurements experience onboard Jason-3 spacecraft," through personal communication with Payan and Sauvaud. The 109 detected spacecraft charging events are listed in the Supplementary Material. Finally, less than 2% of events could not be attributed to spacecraft charging or other natural environment signatures and were therefore excluded.

A typical example of a spacecraft charging event is found on January 13, 2017 within the time interval from 10:27 to 10:31 (see Fig. 1). The satellite charging leads to the formation of a narrow ion band with enhanced ion count rates, as shown within the white ellipse in Fig. 1(b). No ions can be detected below these accelerated ions. Note the intense precipitation of electrons accompanying the charging event. An approximate satellite electric potential can be directly deduced from the energy of the ion low-energy band, which results from the acceleration of ions by the spacecraft potential. Here, the ion signature is measured from 10:28:26 to 10:30:10 for 1 min 44 s. An increase in the high-energy electron counts is detected at 10:27:15–10:30:31 for 3 min 16 s. The maximum ion counts of 5376#, and therefore strongest charging, are found at the energy range of 120.64–199.13 eV (energy channel numbers 11 and 12). Elevated count rates of 2224# are also detected at the energy range 199.13–328.71 eV at 10:29:42, which is the highest ion energy level with a substantial increase in the ion count rate that is clearly related to the charging event.

The longest ion signature is seen in the spacecraft charging event on April 20, 2017, 18:20:04 [see Fig. 1(d)]. It lasts from 18:20:03 to 18:23:36 for 3 min 33 s. A count rate increase in the electron energies is detected between 18:19:48 and 18:23:11, a duration of 3 min 23 s [see Fig. 1(c)]. The electron count rate starts to increase earlier than that detected in the ion spectrum, which is commonly observed. This is expected from the dynamic of charging corresponding to the collection of energetic electrons resulting in a negative platform potential able to accelerate ions toward the spacecraft. The maximum ion counts 12 100# are detected at the energy range of 328.71–542.59 eV at 18:21:02.

It must be stressed that electrons are decelerated by a negatively charged spacecraft before reaching the detector [12]. The real electron energy inside the plasma is thus equal to the measured energy plus the satellite potential. Finally, using the method described above, a total of 109 spacecraft charging events were detected. The time intervals and the maximum ion energy for each charging event are listed in Supplementary Material A. These events were used for the statistical study presented in Section IV.

IV. Statistical Study

The detected events are used for statistical analyses of the event location (magnetic local time (MLT) and invariant latitude), duration (for ions and electrons), spacecraft charging level, and event detection level.

First, we selected all time intervals when good quality measurements have been obtained. Note that telemetry restrictions lead to some missing parts of Jason-3 orbits. This means that more events are to be expected in flight but are not recorded due to lack of data and differential charging not observed by AMBRE. These data are further referred to as the general dataset. The characteristic of the spacecraft charging events dataset is then compared to the characteristics of the general dataset, in order to avoid a bias generated by time intervals where no data could be recorded.

A. MLT and Invariant Latitude Distributions

The distribution of MLT for the general dataset is shown in Fig. 2(a), which shows that the data cover all MLT

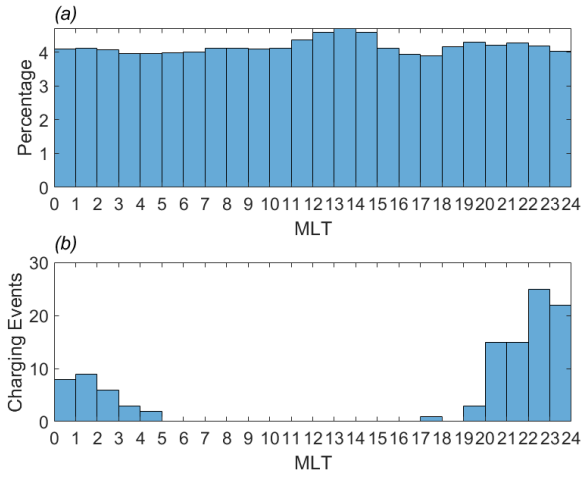

Fig. 2. (a) MLT distribution of the general dataset in percentage per 1-h bin. The distribution is fairly even. (b) Number of charging events detected in each MLT sector.

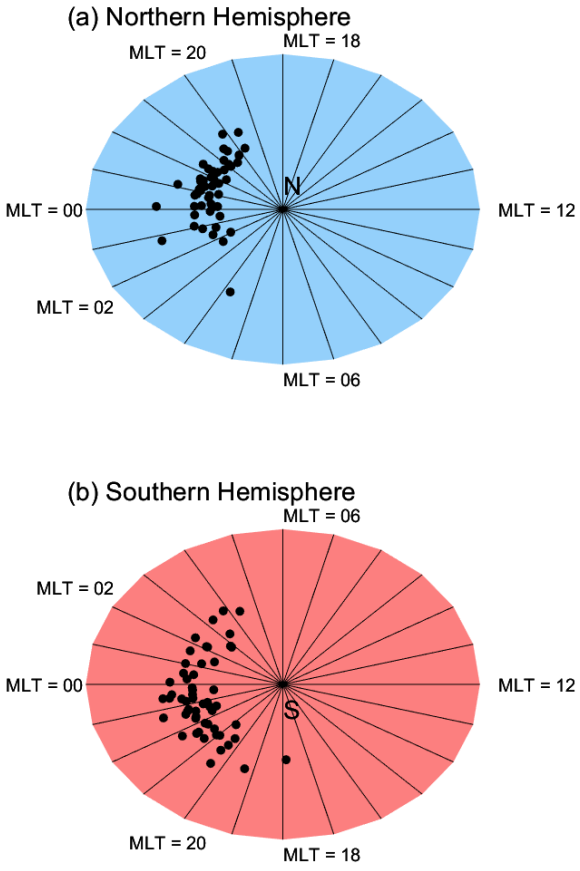

Fig. 3. (a) MLT sector position of spacecraft charging events that were detected in the northern hemisphere. (b) MLT sector position of spacecraft charging events that were detected in the southern hemisphere. The majority of the spacecraft charging events are found between 20h and 02h MLT. The data points appear radially spread for a better representation, but their locations do not correspond to a given latitude.

sectors evenly. Even though the measurements are evenly distributed in MLT, spacecraft charging events are only found on the nightside, between 17h and 05h MLT, predominantly

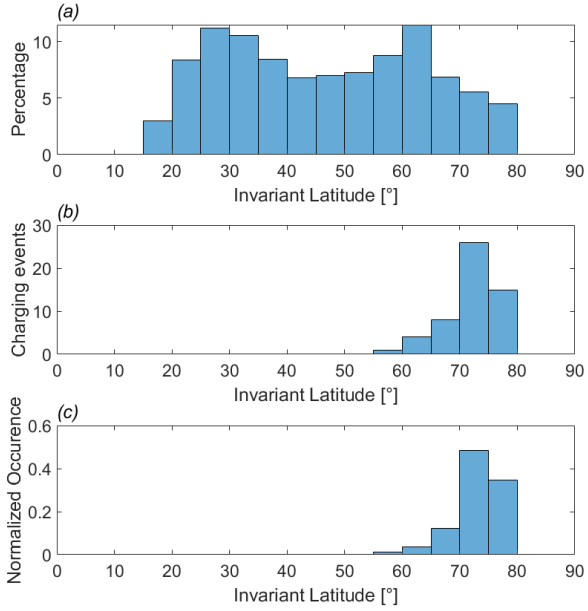

Fig. 4. (a) Invariant latitude distribution of the general dataset in percentage per 5° bin. The distribution only covers 15°–80°. (b) Number of charging events detected in each invariant latitude sector. (c) Normalized spacecraft charging events, i.e., the number of events divided by the general distribution normalized. This emphasizes the occurrence of spacecraft charging events in auroral latitudes 70°–80°.

in the 22h–00h sector, as shown in Figs. 2(b) and 3. The peak is in sector 22h–23h MLT. This is probably due to the high-energy electron precipitation enhancement on the nightside of Earth, associated with substorms. The observed distribution of MLT confirms the results from earlier studies by Gussenhoven *et al.* [2], Wahlund *et al.* [3], Anderson [4], Meng *et al.* [5], Frooninckx and Sojka [7], and Eriksson and Wahlund [13]. The distribution of events is equally divided in the northern and southern hemispheres (55 events north and 55 events south), see Fig. 3.

The invariant latitude distribution for the general dataset is shown in Fig. 4(a), which displays a nonuniform distribution. The dominant part of the dataset is between 15° and 80°. The spacecraft charging events are located in the latitude range of 55°–80° and predominately in the 70°–80° range [see Fig. 4(b)]. This latitude distribution is also in good agreement with the results from earlier studies by Gussenhoven *et al.* [2], Wahlund *et al.* [3], Anderson [4], Meng *et al.* [5], Frooninckx and Sojka [7], and Eriksson and Wahlund [13].

B. Event Duration at the Jason-3 Orbit

We also study the duration of each observed spacecraft charging event (see Fig. 5). A rough estimate of the event duration for ions and electrons was determined "by eye." Occasionally, only a part of the charging was recorded, and occasionally, only a part of the spectra was clear; therefore, the number of events to study the duration was reduced to the ones with clear onsets and decays signatures. Of the 109 events, 86 ion signatures and 61 electron signatures are used to

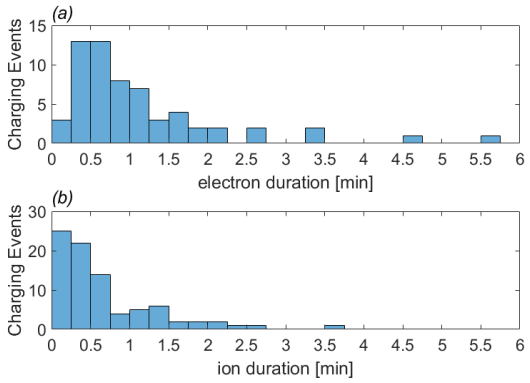

Fig. 5. Duration of (a) electron and (b) ion spacecraft charging signatures. The spacecraft charging events commonly last shorter than 1 min. The electron signature duration peaks between 15 and 45 s and the ion signature duration peaks under 130 s. Note that the difference comes from the fact that only the portion of electron auroral precipitation with an average energy higher than 4–5 keV is able to charge the satellite.

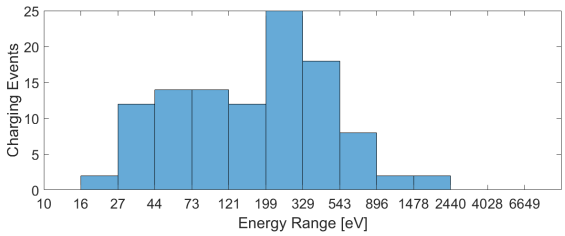

Fig. 6. Ion energy level with the strongest charging was detected for all 109 events. The peak lies between 199 and 543 eV.

determine the duration. The ion signature predominately lasts under 30 s, as shown in Fig. 5(b). In the ion signature, only two events are found to last over 2 min 30 s, namely on January 25, 2017, lasting from 03:30:34 to 03:33:14, and April 20, 2017, lasting from 18:20:03 to 18:23:36. In both cases, the electron signatures last for a similar time span of ±10 s. In comparison, the peak of the electron signature duration is found in between 30 s and 1 min, as shown in Fig. 5(a). In the electron signatures, only two events last over 4 min 30 s. The two events are on September 8, 2017, from 00:24:50 to 00:29:15, and on January 3, 2020, from 07:16:54 to 07:21:32 with ion signatures from 1 min 30 s to 2 min. The observed event durations depend on how long time the spacecraft spends in auroral regions and with this on the orbit. Hence, the detected durations are specifically for the Jason-3 orbit. However, the detected durations are in gross agreement with results from earlier studies by Gussenhoven *et al.* [2], Wahlund *et al.* [3], and Anderson [4], [14], which can be expected as charging timescales (especially ions signatures duration) are strongly driven by specific spacecraft characteristics (e.g., external surfaces materials) in addition to orbital position (e.g., altitude) when crossing auroral regions. Such dependence will be addressed in a later study.

C. Maximum Charging Distribution

The ion energy level with the highest count rate was detected and is shown in Fig. 6. The energy level of strong spacecraft charging for count rates $>10^3$# is noted.

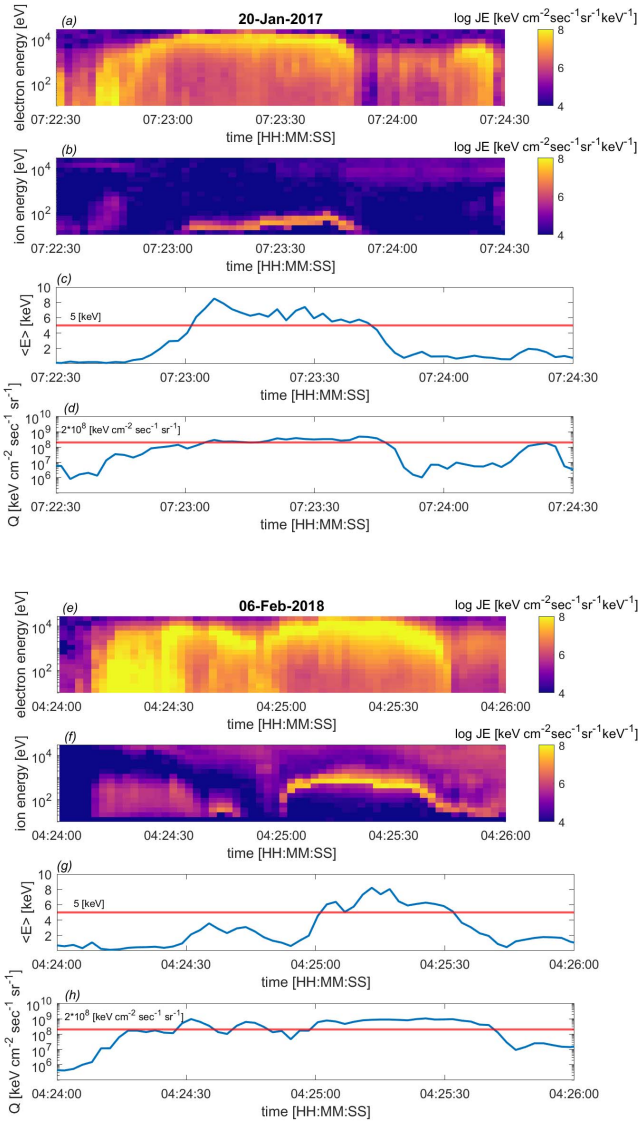

Fig. 7. (a)–(d) Weak and (e)—(h) strong spacecraft charging event. Energy-time spectrograms of electrons are plotted in (a) and (e) and of ions in (b) and (f). The electron average energy and the electron integral energy fluxes are plotted below the spectrograms in (c) and (g) and (d) and (h), respectively. The horizontal red lines indicate an 5 keV average energy and an integral energy flux level corresponding to 2×10^8 keVcm^{-2}s^{-1}sr^{-1}.

The histogram of the strongest ion charging levels is shown in Fig. 6. For this figure the 16-energy-channel resolution is used. The peak lies between 199.13 and 328.71 eV.

One of the stronger events, on February 6, 2018, charges up to between 328.7 and 542.59 eV with the count rates of 12 160# at 04:25:27 [see Fig. 7(e)–(h)]. A spacecraft charging event with a low ion charging level (between 26.83 and 44.28 eV) on January 20, 2017 is shown in Fig. 7(a)–(d), and the count rates reach 2632# for this charging level at 07:23:25. In both cases, the average energy [Fig. 7(c) and 7(g)] reaches values in excess of 5 keV, while the integral energy flux [Fig. 7(d) and 7(h)], larger for the February 2018 event than for the January 2017 one, is close to or higher than 2×10^8 keVcm^{-2}s^{-1}sr^{-1}.

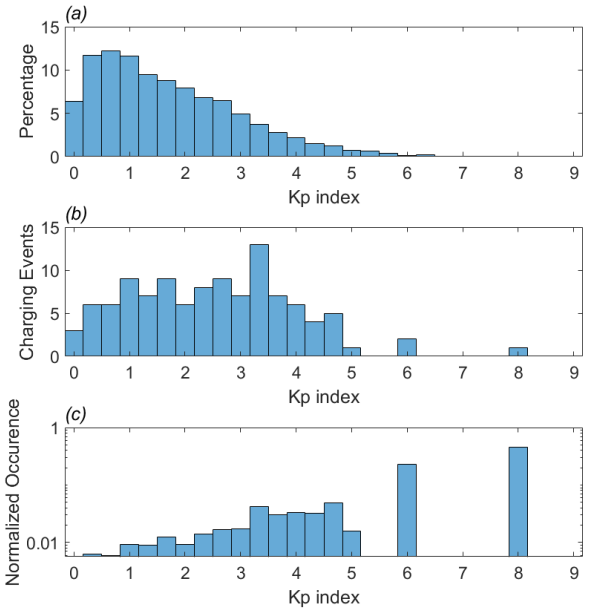

Fig. 8. (a) Kp index distribution for the general dataset. Most of the relevant collected spacecraft data have been collected at low Kp indices. (b) Kp indices for spacecraft charging events. (c) Normalized occurrence (normalized Kp index during spacecraft charging events divided by the general distribution). Here, we can see that even though most of the data are collected at low Kp values, we do encounter a high number of charging events in high Kp values. The probability of encountering conditions leading to charging events is increasing with the Kp index.

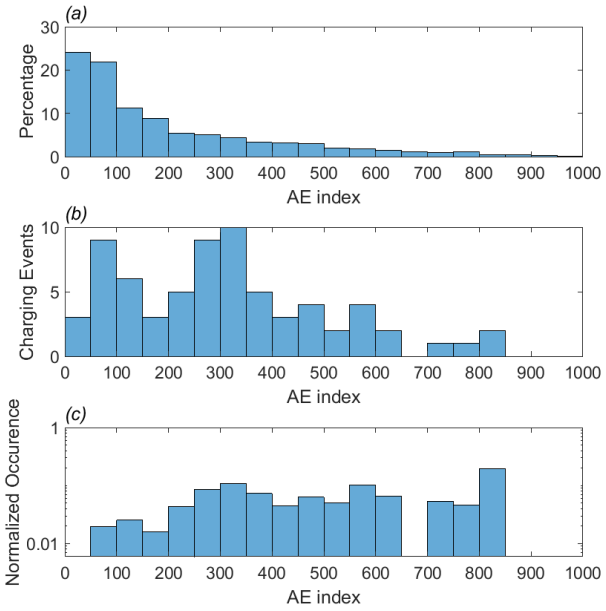

Fig. 9. (a) General AE index distribution. Most of the relevant collected spacecraft data have been collected at low AE indices. (b) AE indices for spacecraft charging events. (c) Normalized occurrence. We do encounter a fair number of charging events in high AE values, even though we do not encounter the conditions very often. The probability of encountering conditions leading to charging events is increasing with the AE index up until AE = 350.

D. Charging Versus Magnetic Activity

The dependence of spacecraft charging events on geomagnetic conditions (Kp and AE indices) is investigated by

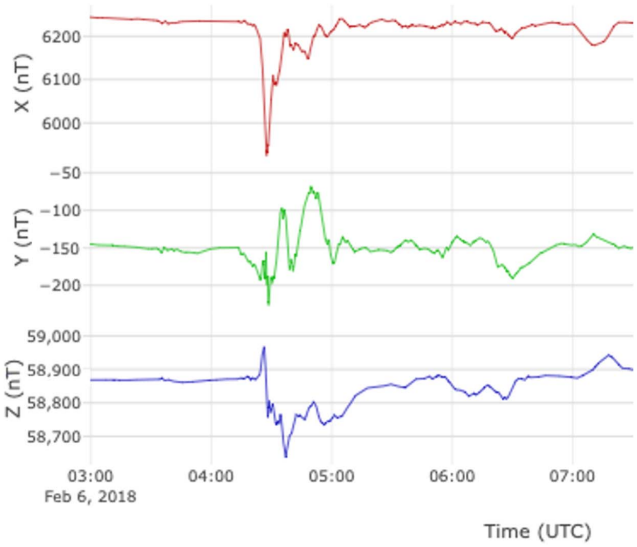

Fig. 10. Spacecraft charging event on February 6, 2018 starting at 04:24:59 UT–04:26:02 UT (geographic latitude: 59.16 and geographic longitude: −74.72) can be correlated with decrease in the Bx component recorded with local magnetometer data at the RANK station (geographic longitude: 62.82 and geographic latitude: −92.11; westward of the spacecraft charging event location) of the CARISMA network. The plot shows the Bx, By, and Bz components, all of them showing disturbances at the spacecraft charging event time. The dip in the Bx component starts at 04:26 UT, peaks at 04:29 UT, and indicates a substorm event.

comparing the natural distribution in the general dataset and the distribution during the events [see Figs. 8 and 9]. The Kp and AE indices are used as a proxy for the energy input from the solar wind to the Earth, where higher indices correspond to larger disturbances. The averages of the Kp and AE indices were not centered at the time of the charging event, but the charging events were placed in the given time range. This is not expected to make a difference in the correlation since the indices give a general proxy of the disturbances in the geomagnetic field and do not provide local information.

To obtain the Kp index, 13 selected subauroral ground-based magnetic observatories are used to derive the mean value of the disturbance levels in the two horizontal field components. The Kp index is provided in a 3-h resolution and is available for all 109 events. Looking at the occurrence of Kp indices in the general dataset, it shows that lower indices are more common than the ones at the higher end [see Fig. 8(a)]. The most frequent Kp indices at spacecraft charging events are between 1 and 3+ [see Fig. 8(b)]. The normalized distribution is shown in Fig. 8(c). It shows an increasing number of spacecraft charging events with increasing Kp index. The small percentage of Kp over 5 in the general dataset does not provide reliable statistics. However, even when excluding these specific events, a clear increase is detected.

The AE index, developed by Davis and Sugiura [15], provides a measure of global electrojet activity. It shows the total range of deviation from quiet day values of the horizontal magnetic field around the auroral oval and is a good measure for substorms. Here, the AE index is used in a 1-h resolution. At the time of writing, the AE index was available until February 28, 2018; therefore, only for 69 events, the AE index is known. The AE index occurrence in the general

TABLE II

TIMINGS OF THE CHARGING EVENTS SHOWN IN FIGS. 11 AND 12. BACKGROUND MEASUREMENT BEFORE THE CHARGING. BEGINNING OF THE CHARGING (E-RISE), AND MAXIMAL CHARGE (I+ PEAK)

Date	13-01-2017	27-01-2017	27-06-2018	25-12-2019	03-01-2020
background	10:24:39	04:11:01	20:13:57	03:59:30	07:12:47
e- rise	10:28:02	04:12:55	20:15:14	04:00:31	07:18:40
i+ peak	10:29:42	04:14:11	20:15:33	04:01:37	07:19:44

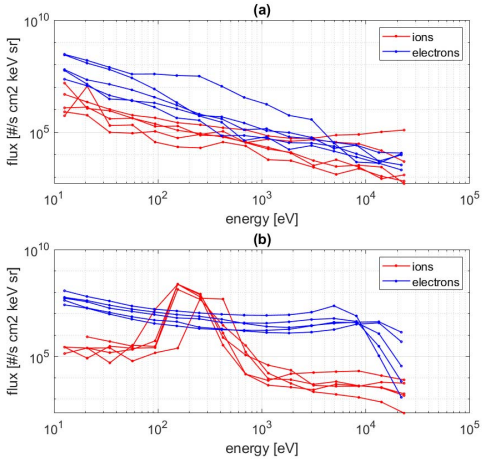

Fig. 11. Five spacecraft charging events with their ion peaks within 120–328 eV are shown. (a) Background flux spectra, profiles before the spacecraft charging events begin. (b) Uncorrected spectra at the spacecraft charging peak times. Note that the figure displays the rough electron spectra measured by AMBER, with no attempt to correct the spectra for deceleration caused by the spacecraft charging.

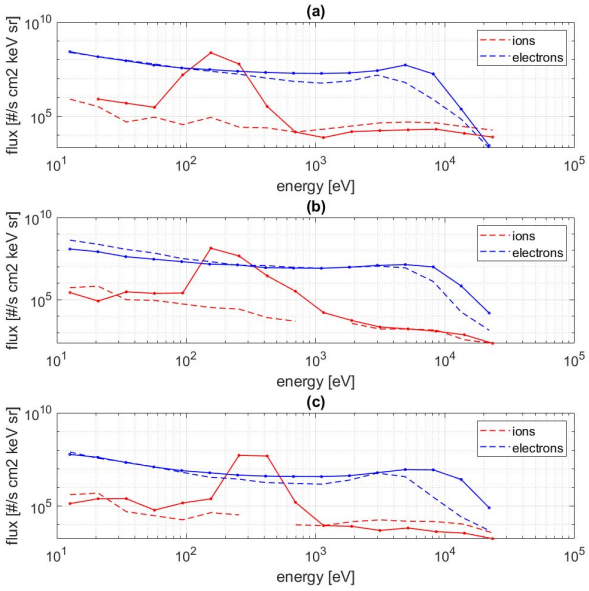

Fig. 12. Electron (blue) and ion (red) flux comparison for electron onset (dashed line) and ion peak (solid line).The dashed lines describe the environment before the charging event is detected and the solid lines describe the environment for the largest ion flux detected during each event. (a) Fluxes from January 13, 2017. (b) Fluxes from June 27, 2018. (c) Fluxes from December 25, 2019. Note that for the dashed spectra occurring before the charging events, no correction of the electron spectra is required, while the electron spectra at the ion peak are shown as uncorrected spectra and are not corrected with regard to the maximum charge for the satellite potential.

dataset is decreasing with the magnitude of the AE index [see Fig. 9(a)]. The AE index at the spacecraft charging events is very variable [see Fig. 9(b)]. The normalized distribution shows a weak correlation on increasing AE index [Fig. 9(c)]. Despite the weak correlation with the 1-h averaged AE index, individual passes over auroral stations showed a nice correlation between spacecraft charging and negative magnetic bays linked to substorm expansion phase and the related short-lived AE enhancement. This can be seen by looking at, e.g., a spacecraft charging event on February 6, 2018 starting at 04:24:59 UT–04:26:02 UT correlated with magnetometer data in its vicinity, which measured a decrease of about 300 nT in the Bx component (see Fig. 10). The 1-h index may not be in sufficient resolution to detect short-lived effects.

V. FLUX SPECTRA AND INTEGRAL PARAMETERS

To characterize charging events, the differential flux is inspected by stepping through the differential flux energy profiles for different times. In Fig. 11(a), typical spectra before spacecraft charging events are shown. Here, five subsequent spacecraft charging events (see Table II) have been selected for further analysis and grouped for comparison. For these events, ion energies are peaking at around 120–328 eV [see Fig. 11(b)]. As the flux of high-energy electrons increases, as shown in Fig. 11(b) (blue lines), the spacecraft charges negatively and the low-energy ions are accelerated toward the negatively charged spacecraft, resulting in the observed ion spectra with a well-defined energy peak.

Fig. 12 shows in more detail for three selected charging events the change of the electron energy flux at the beginning of each event and the core of the charging event. It appears that there is an increase in the electron high-energy fluxes, which corresponds to the maximum charge measured with the ion measurements performed onboard Jason-3. Here, the measured differential flux spectra must be corrected to account for spacecraft charging. The electron energy has to be modified to consider the electron deceleration resulting from the satellite negative charging. This precludes any electron measurements with energies lower than the spacecraft charge, these particles being repelled from the AMBER detector. The fluxes are corrected according to the Liouville theorem, as described in the following equation:

$$f_c = f_m \times \left(1 + \frac{U}{E}\right) \tag{1}$$

where U is the negative satellite potential, f_m is the apparent flux detected at the energy E_m both measured internally by the AMBER, and f_c is the corrected flux at the plasma energy $E_m + |U|$. For example, for a spacecraft charge of -100 V, electrons with energies in the plasma lower than 100 eV cannot

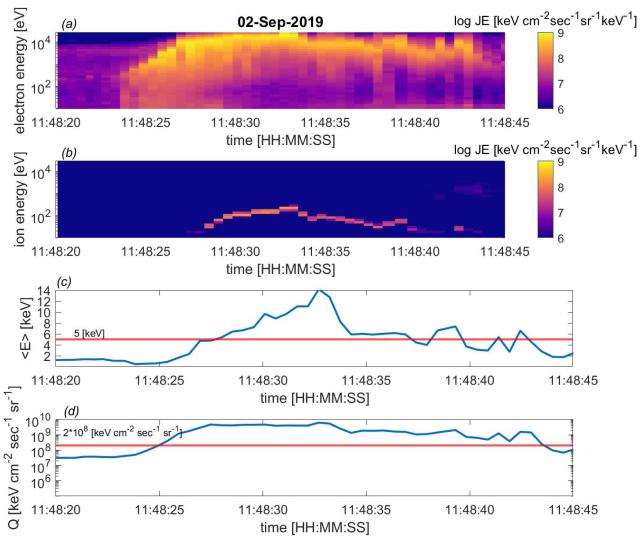

Fig. 13. Energy flux versus energy and time plot on September 2, 2019 between 11:48:20 and 11:48:45. The two top panels show the energy–time electron spectrogram and energy–time ion spectrogram. The two bottom panels display the average energy and integral energy flux of electrons. The horizontal red lines indicate an 5 keV average energy and an integral energy flux level corresponding to 2×10^8 keVcm^{-2}s^{-1}sr^{-1}.

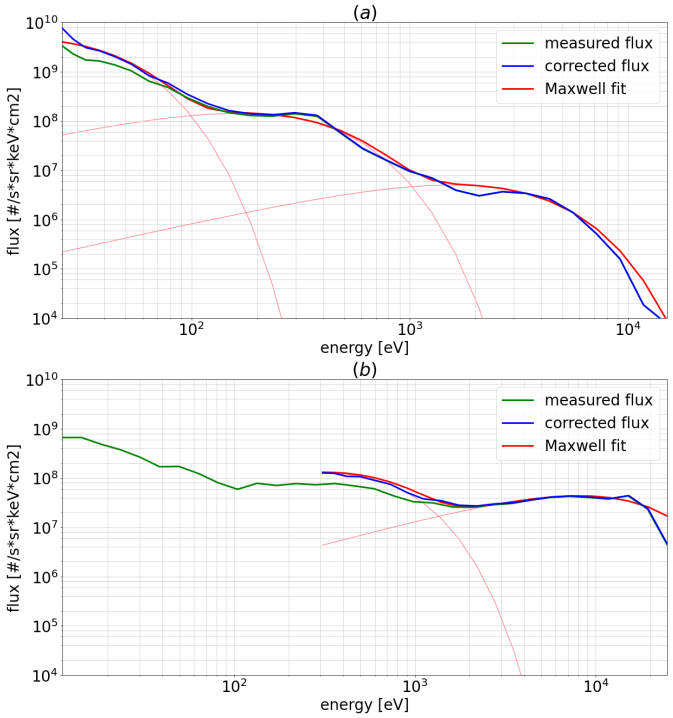

Fig. 14. Energy spectra for the spacecraft charging event on September 2, 2019. (a) Spectrum at 11:48:24 UT, corresponding to the electron flux increase preceding the charging event. (b) Energy spectra at the ion energy peak at 11:48:31 UT. The green line shows the Amber measurements before corrections for charging effects. The blue line is for the corrected spectrum taking into account the absence of low-energy electrons repelled by the spacecraft. The red lines show the Maxwellian fits of the corrected spectrum, indicating temperatures of 299 and 8127 eV and densities of 2 and 1 cm^{-3}. The fit does not give detailed information about ionospheric conditions and corresponding electron populations, but gives a good indication of the environmental changes needed to produce the charging events.

be measured. The electrons with an apparent energy of 10 eV have a real energy of 110 eV inside the plasma, far from the spacecraft, and their flux must be corrected using (1).

To adequately model the charging environment, one can perform a fitting procedure of the electron energy spectra using bi-Maxwellian and triple-Maxwellian distributions. We provide such an example of fittings for the charging event measured on September 2, 2019 whose general features are given in Fig. 13. We attempt to derive a fitting procedure using bi-Maxwellian and triple-Maxwellian distributions. The time of the electron rise and at the ion peak has been chosen for the fit [see Fig. 14(a) and (b), respectively]. The measured differential flux spectrum f_m has been corrected according to (1), with f_c being the corrected flux spectrum, U the spacecraft potential, and E the energies at which the differential flux is measured. The high-energy Maxwellian for the population at the electron rise corresponds to an electron temperature of 1573 eV and an electron density of 0.1 cm^{-3}. The bi-Maxwellian populations for the ion peak correspond to electron temperatures of 299 and 8127 eV and electron densities of 1 and 2 cm^{-3}. This means that when comparing the characteristics of the hot electron component preceding the charging event [Fig. 14(a)] to the one at the ion energy peak [Fig. 14(b)], we see that the temperature has increased by around a factor of 5 and the electron density around a factor of 10. The fits do not give information about ionospheric conditions and corresponding electron populations but can be used to reproduce the data presented in Fig. 14.

Fitting some of our most severe events with a Fontheim distribution has shown that none of them exceed the worst-case environment. Two of the electron flux spectra of events where the spacecraft charges to potentials more negative than −1000 V are shown as examples in Fig. 15 in comparison to a Fontheim distribution. The electron fluxes at the ion peaks do not exceed the European Cooperation for Space Standardization (ECSS) worst-case spectral distributions.

Spectrum fitting is a useful method to characterize the plasma environment leading to spacecraft charging. It is also useful to derive parameters allowing to later model such an auroral environment in dedicated charging codes. However, a simpler and quicker method can also be used: the calculation of the electron average energy and integral energy flux [Figs. 7 and 13]. Every charging event corresponds to average energies higher than 4–5 keV and integral energy fluxes higher than 2×10^8 keVcm^{-2}s^{-1}sr^{-1}. When these simple values are computed onboard, a warning can be sent to the platform units, including sensitive payloads, as thresholds are reached. This can possibly be useful to mitigate in real-time detrimental surface charging effects encountered during space weather events.

VI. Discussion

Spacecraft charging and possibly associated electric breakdown present a substantial risk to the health of spacecraft orbiting Earth, where the ambient plasma is relatively tenuous. During magnetospheric perturbations, high fluxes of energetic electrons can cause substantial spacecraft surface charging. In this report, we have investigated charging events detected in the Jason-3/Amber data. In total, 109 clear spacecraft charging

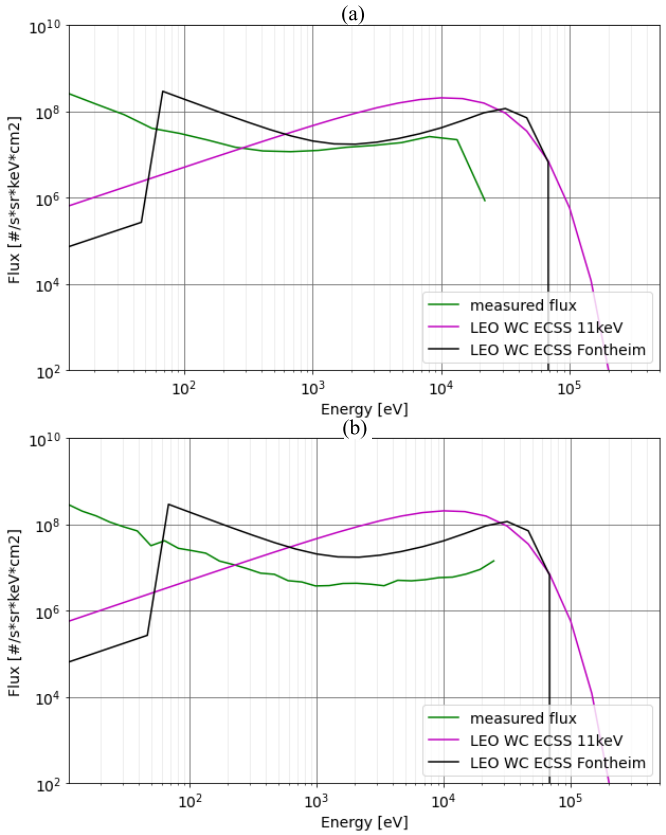

Fig. 15. (a) Electron flux (shown in green) of the charging event on January 25, 2017 03:30:34 UT–03:33:14 UT at the ion peak. (b) Electron flux (shown in green) of the charging event on July 25, 2017 20:56:08 UT–20:56:26 UT at the ion peak. This is compared with an ECSS worst-case Fontheim distribution (shown in black) and an 11 keV flux (shown in violet). The electron flux peak for this event is out of the measurement range of AMBRE. The explored cases do not exceed the worst-case distributions.

events were found, with the largest spacecraft potential in excess of 2000 V negative. All spacecraft charging events show a well-defined peak structure that we expect from a charging event in the count rates' time evolution. These charging events were first automatically detected in the database and then confirmed visually. Finally, in our study, the majority of the events are found in 2017.

Over this short three years data period, we find peaks of spacecraft charging events in the months December–February and June–August. The duration of the charging event is predominantly under 30 s, with only a few events lasting longer than 1 min 30 s (see Fig. 5). The duration is comparable to the average time spent by the spacecraft in the discrete auroral zone.

According to Gussenhoven *et al.* [2], the primary driver for the occurrence frequency of charging events on the DMSP spacecraft and the solar cycle dependence is the requirement that the ambient density must be below about 10^4 cm^{-3}. Similar conditions are likely in the case of Jason-3, as inverted V structures are well known to be depleted with thermal plasma. However, we have no direct measurements of the plasma background density to correlate with.

Most of the spacecraft charging events on Jason-3 show charging to -30 V to -1 kV, with the highest detectable spacecraft potential being -10 V; 28 spacecraft charging events are above -100 V, 77 are in between -100 V and -1 kV, and 4 are below -1 kV, as shown in Fig. 6. This is comparable to the DMSP and Freja satellites. A difference in charging levels may be due to the altitude of the Jason-3 satellite. Indeed, the DMSP altitude is at 850 km and Jason 3 is at 1336 km, so DMSP is flying into regions of higher plasma densities. Spacecraft design is clearly another contributor to differences in observed charging levels. A weak correlation of the hourly AE index and spacecraft charging event occurrence is shown up to AE $=$ 350, see again Fig. 9. The spacecraft charging events are peaking between an AE index of 300 and 350. Above this threshold, no clear correlation can be seen between the occurrence of spacecraft charging events and an increased AE index. Short-lived substorm events with expansion phases of 20–30 min may not affect the hourly AE index, and this is why the correlation may seem weak. However, when looking at individual cases with local magnetometer measurements, a correlation between substorms and spacecraft charging events is more dominant, see again Fig. 10. Regarding the Kp index, the spacecraft charging events occur more frequently at higher Kp indices (Fig. 8). However, the distribution shows some larger trend for Kps in the range 4–5, which should be further studied. The spacecraft charging events are found in the MLT sector 17h–5h, predominantly in the 20h–00h sector [see Figs. 2 and 3]. This is probably due to high-energy electrons enhancements in the midnight sector. Note that all the spacecraft charging events, but one, are found on the nightside.

On Jason-3, 22 charging events (20%) were observed in sunlit conditions and 87 (80%) in shade. On Freja, sunlit events were rare and most charging was observed in eclipse [8]. On DMSP, no charging in sunlit conditions was recorded [2]. This may be due to a lower ambient ion density for the higher altitudes of Jason-3 in comparison to the other satellites.

Both DMSP and Freja data are in general in good agreement with the above results deduced from AMBER onboard Jason-3. Furthermore, inspecting the latitude distribution of spacecraft charging events, we find that spacecraft charging events are detected in between 55° and 80° invariant latitude (shown in Fig. 4, in agreement with previous studies (see [5], [8]).

Comparisons between flux measurements recorded before and during charging events, as shown in Figs. 12 and 14, are useful to understand the changes in the environment that cause strong charging events. The energy spectra are to be further investigated to derive characteristic electron temperature and density values of the auroral electron component responsible for the spacecraft charging. This requires energy spectra correction to account for the effect of the charged spacecraft on the measured particles. In this article, we have shown that the electron average energy and integral energy flux, computed from successive electron spectra, could provide a valuable way to predict the charging events. The use of an energy threshold above which these integral values are computed allows to avoid, in first approximation, the corrections induced by the satellite potential. Charging events only occur for an average energy above 4–5 keV and for an integral energy flux at least equal to 2×10^8 keVcm^{-2}s^{-1}sr^{-1} [see Figs. 7 and 13].

Furthermore, we have shown that the Fontheim distribution is in our case a valid tool to model the worst-case environment as it is not exceeded for the studied events on Jason-3 (see again Fig. 15). However, the current state of the analysis does not exclude the possibility to find more severe events that may exceed the worst-case environment.

VII. Conclusion

This study provides an analysis of spacecraft charging events at low altitudes using AMBER data on the Jason-3 satellite. Plasma environment conditions leading to negative spacecraft charging were investigated and 109 spacecraft charging events were found. All spacecraft charging events are associated with electron inverted "V" structures. At the Jason-3 orbit, the ion signature predominately lasts under 30 s, while the electron signature lasts between 30 s and 1 min. The charging events generally begin only when the electron average energy exceeds 4–5 keV.

1) The ion signature predominately lasts under 30 s, while the electron signature lasts between 30 s and 1 min.
2) During most of the studied spacecraft charging events, Jason-3 charges to potentials between -30 V and -1 kV. The spacecraft charging event with the highest detected ion energy was found in the ion energy channel of 2440.31 eV. This is comparable to the largest frame potential observed onboard the DMSP satellite, however, at lower altitude, suggesting a strong impact on the local plasma density since the corresponding electrons energy flux leading to DMSP event was likely larger than that observed by Jason-3 during this event.
3) The hourly AE index correlation is rather weak and only visible up to an AE of 350. Local magnetometers, however, do show a correlation with the observed spacecraft charging events on Jason-3.
4) The Kp index correlation clearly shows an increasing number of spacecraft charging events with an increasing Kp index.
5) Almost all spacecraft charging events are found in the MLT sector 17h–05h, predominately just before midnight.
6) The distribution is identical between the northern and southern hemispheres.
7) All spacecraft charging events are found within the invariant latitude range from 55° to 80°.
8) The most severe of the detected events does not exceed the worst-case environment (Fontheim distribution) in our analysis. However, it cannot be excluded that more severe events, which are not included in our study, may exceed the worst-case environment.

The energy spectra are to be further investigated to retrieve plasma parameters and characterize the plasma environment conditions in more detail. The nice correlation found between the satellite electric potential profile and the auroral electron average energy can be used to infer some interesting charging properties. An electron average energy above about 4–5 keV and an association with high-energy fluxes is necessary for the satellite charging to occur. Such an electron characteristic energy and high fluxes are only achieved in discrete auroral forms or inverted V. As models of the auroral electron average energy (temperature) become available, they will be used to predict spacecraft charging events in the nightside sector of the auroral oval. Another important conclusion comes from the fact that charging events are collocated with inverted V events. These structures are produced by field-aligned potential drops accelerating electrons at altitudes of several thousands of kilometers. Above these altitudes, the field-aligned source electron average energy is weaker and no strong satellite potentials are expected to occur. Furthermore, at these high altitudes, a spacecraft with a high inclination, i.e., crossing auroral field lines, will be in daylight. UV fluxes will produce a strong emission of photoelectrons relaxing the satellite charge.

Data Availability

The AMBER scientific data and Jason-3 ephemeris are downloaded from http://clweb.irap.omp.eu/. The hourly AE index is downloaded from http://wdc.kugi.kyoto-u.ac.jp/dstae/index.html, and the 3-h Kp index from http://wdc.kugi.kyoto-u.ac.jp/kp/index.html. The magnetometer data from the RANK station of the CARISMA network are accessed from https://www.carisma.ca/carisma-data-repository.

References

[1] E. C. Whipple, "Potentials of surfaces in space," *Rep. Prog. Phys.*, vol. 44, no. 11, pp. 1197–1250, 1981.
[2] M. Gussenhoven, D. Hardy, F. Rich, W. Burke, and H.-C. Yeh, "High-level spacecraft charging in the low-altitude polar auroral environment," *J. Geophys. Res.: Space Phys.*, vol. 90, no. A11, pp. 11009–11023, 1985.
[3] J.-E. Wahlund *et al.* (1999). *Analysis of Freja Charging Events: Statistical Occurrence of Charging Events*. [Online]. Available: https://www.space.irfu.se/aie/publ/Wahlund1999b.pdf
[4] P. C. Anderson, "Characteristics of spacecraft charging in low Earth orbit," *J. Geophys. Res.*, vol. 117, p. A07308, 2012, doi: 10.1029/2011JA016875.
[5] X. Meng, D. Chen, L. Shi, S. Liu, and S. Chen, "Statistical study of surface-charging events in aurora region over one solar cycle," *IEEE Trans. Plasma Sci.*, vol. 47, no. 8, pp. 3942–3946, Aug. 2019.
[6] L. A. Frank and K. L. Ackerson, "Observations of charged particle precipitation into the auroral zone," *J. Geophys. Res.*, vol. 76, no. 16, pp. 3612–3643, Jun. 1971. [Online]. Available: https://agupubs.onlinelibrary.wiley.com/doi/abs/10.1029/JA076i016p03612
[7] T. B. Frooninckx and J. J. Sojka, "Solar cycle dependence of spacecraft charging in low Earth orbit," *J. Geophys. Res.: Space Phys.*, vol. 97, no. A3, pp. 2985–2996, Mar. 1992.
[8] J.-E. Wahlund, L. Wedin, A. Eriksson, B. Holback, and L. Andersson. (1999). *Analysis of Freja Charging Events: Charging Events Identification and Case Study*. [Online]. Available: https://www.space.irfu.se/aie/publ/Wahlund1999a.pdf
[9] B. Lavraud *et al.*, "AMBRE: A compact instrument to measure thermal ions, electrons and electrostatic charging onboard spacecraft," in *Proc. ESA Workshop Aerosp. EMC (Aerospace EMC)*, May 2019, pp. 1–5.
[10] J.-A. Sauvaud and D. Payan, "Résultats préliminaires de l'expérience de mesure des particules ambre installée à bord du satellite Jason-3," CNES, Toulouse, France, Tech. Rep. DSO/TB/EL/2017-15526, 2017.
[11] J.-A. Sauvaud, D. Delcourt, M. Parrot, D. Payan, T. Raita, and E. Penou, "Low-altitude observations of recurrent short-lived keV ion microinjections inside the diffuse auroral zone," *J. Geophys. Res.: Space Phys.*, vol. 123, no. 3, pp. 2054–2063, Mar. 2018.
[12] B. Lavraud and D. E. Larson, "Correcting moments of *in situ* particle distribution functions for spacecraft electrostatic charging," *J. Geophys. Res.: Space Phys.*, vol. 121, no. 9, pp. 8462–8474, Sep. 2016.
[13] A. I. Eriksson and J. E. Wahlund, "Charging of the Freja satellite in the auroral zone," *IEEE Trans. Plasma Sci.*, vol. 34, no. 5, pp. 2038–2045, Oct. 2006.

[14] P. C. Anderson, "A survey of surface charging events on the DMSP spacecraft in LEO," in *Proc. Spacecraft Charging Technol., 7th Int. Conf.*, 2001, pp. 331–336.
[15] T. N. Davis and M. Sugiura, "Auroral electrojet activity index AE and its universal time variations," *J. Geophys. Res.*, vol. 71, no. 3, pp. 785–801, Feb. 1966.

Florine Enengl received the M.Sc. degree in electrophysics from the KTH Royal Institute of Technology, Stockholm, Sweden, in 2019. She is currently pursuing the Ph.D. degree in space plasma physics with the University of Oslo, Oslo, Norway. Her research interests include particle precipitation, ionospheric scintillation, Langmuir probes, and spacecraft charging.

Mika K. G. Holmberg is currently a Researcher with the Planetary Magnetospheres Research Group, Dublin Institute for Advanced Studies (DIAS), Dublin, Ireland. Her work focuses on the studies of plasma structures and dynamics in the magnetospheres of Saturn, Mars, and Jupiter. She also develops analysis codes for Langmuir probe measurements and studies spacecraft charging and its impact on particle and field measurements.

Fabrice Cipriani is currently a Space Environment and Effects Analyst at the Space Research and Technology Center (ESTEC), European Space Agency (ESA), Noordwijk, The Netherlands. He is working in the field of spacecraft–plasma interactions, plasma and neutral environment modeling, and environment payloads development. He is chairing the Spacecraft Plasma Interaction Network in Europe.

Jean-André Sauvaud is currently the Research Director Emeritus at CNRS, Institut de Recherche en Astrophysique et Planétologie (IRAP), Toulouse, France, where he is leading the realization of numerous space instrumentations, including the STEREO and the Bepi Colombo-MMO electron instruments and the initial design of the AMBRE ion and electron sensors flown onboard Jason-3. He was the Principal Investigator of the AMBRE instrument.

Denis Payan is currently a Senior Expert at the Centre Nationale d'Etudes Spatiales (CNES), the French Space Agency, Toulouse, France. He was specialized in spacecraft charging, electrostatic discharges, high voltages, and arcing phenomenon. He was the Project Manager of the AMBER plasma monitor. He is now in charge of radio frequency high-power effects.

Jean-Charles Matéo-Vélez is currently a Research Engineer with ONERA—The French Aerospace Lab, Toulouse, France, where he is specialized in the fields of spacecraft charging and electrostatic discharges. He is in charge of modeling spacecraft plasma interactions, both numerically and experimentally, and is involved in mitigation techniques.

Angelica Sicard is currently a Research Engineer with ONERA—The French Aerospace Lab, Toulouse, France, where she is specialized in the field of radiation belts modeling. She is in charge of analyzing *in situ* data and developing specification models for space industries.

Benoît Lavraud is currently the Research Director of CNRS, Institut de Recherche en Astrophysique et Planétologie (IRAP), Toulouse, France. He is an expert in space plasma physics and solar-terrestrial interactions. He is or has been involved in the science or the instrumentation of projects, such as Cluster, STEREO, AMBRE, MMS, Parker Solar Probe, Solar Orbiter, Comet Interceptor, and HelioSwarm.t.